doi:10.1093/plcell/koaa043

THE PLANT CELL

THE PLANT CELL 2021: 33: 475–491

Large-Scale Biology

Photoperiod-responsive changes in chromatin accessibility in phloem companion and epidermis cells of Arabidopsis leaves

Hao Tian [1,†] Yuru Li [1,†] Ce Wang,[1,†] Xingwen Xu [1,†] Yajie Zhang,[1] Qudsia Zeb,[1] Johan Zicola [2] Yongfu Fu [3] Franziska Turck [2] Legong Li [1] Zefu Lu [3,*,‡] and Liangyu Liu [1,*,‡]

1 Beijing Key Laboratory of Plant Gene Resources and Biotechnology for Carbon Reduction and Environmental Improvement, and College of Life Sciences, Capital Normal University, Beijing 100048, China
2 Max Planck Institute for Plant Breeding Research, Cologne, D-50829, Germany
3 National Key Facility of Crop Gene Resource and Genetic Improvement, Institute of Crop Sciences, Chinese Academy of Agricultural Sciences, Beijing 100081, China

*Author for correspondence: liangyu.liu@cnu.edu.cn (L.L) and luzefu@caas.cn (Z.L.)
†These authors contributed equally to this work.
‡Senior authors.

L.Y.L. designed the experiments. Y.R.L., H.T., and C.W. performed most of the experiments such as ATAC-seq, RNA-seq, gene transformation, and phenotyping. Z.F.L. carried out most of the bioinformatic analysis and H.T. helped to prepare the figures. X.W.X., Y.J.ZH., J.Z., and Q.Z. helped to generate materials and carry out genotyping and phenotype analysis. L.Y.L., Z.F.L., and L.G.L. drafted the manuscript, and F.T. and Y.F.F. gave advice and revised the manuscript.

The author(s) responsible for distribution of materials integral to the findings presented in this article in accordance with the policy described in the Instructions for Authors (https://academic.oup.com/plcell/pages/General-Instructions) is: Liangyu Liu (liangyu.liu@cnu.edu.cn).

Abstract

Photoperiod plays a key role in controlling the phase transition from vegetative to reproductive growth in flowering plants. Leaves are the major organs perceiving day-length signals, but how specific leaf cell types respond to photoperiod remains unknown. We integrated photoperiod-responsive chromatin accessibility and transcriptome data in leaf epidermis and vascular companion cells of *Arabidopsis thaliana* by combining isolation of nuclei tagged in specific cell/tissue types with assay for transposase-accessible chromatin using sequencing and RNA-sequencing. Despite a large overlap, vasculature and epidermis cells responded differently. Long-day predominantly induced accessible chromatin regions (ACRs); in the vasculature, more ACRs were induced and these were located at more distal gene regions, compared with the epidermis. Vascular ACRs induced by long days were highly enriched in binding sites for flowering-related transcription factors. Among the highly ranked genes (based on chromatin and expression signatures in the vasculature), we identified *TREHALOSE-PHOSPHATASE/SYNTHASE 9* (*TPS9*) as a flowering activator, as shown by the late flowering phenotypes of T-DNA insertion mutants and transgenic lines with phloem-specific knockdown of *TPS9*. Our cell-type-specific analysis sheds light on how the long-day photoperiod stimulus impacts chromatin accessibility in a tissue-specific manner to regulate plant development.

Received October 30, 2020. Accepted November 29, 2020. Advance access publication January 4, 2021

Introduction

Flowering time is an important contributor to reproductive success and fitness of higher plants (Huijser and Schmid, 2011). Many different pathways including the photoperiod (day length), gibberellin acid, vernalization (a period of cold), thermo-sensory, autonomous, sugar, and aging pathways play critical roles in the regulation of flowering time in *Arabidopsis thaliana* (Arabidopsis) (Putterill et al., 2004; Turck et al., 2008; He, 2009; Wang et al., 2009; Wu et al., 2009; Andres and Coupland, 2012; Kumar et al., 2012; Wahl et al., 2013).

In the photoperiod pathway, transcription of *CONSTANS* (*CO*) is activated by GIGANTEA-mediated degradation of transcriptional repressors of the CYCLING DOF FACTOR (CDF) family (Imaizumi et al., 2005; Sawa et al., 2007; Fornara et al., 2009; Cheng et al., 2019). Under long days (LDs), CO, NUCLEAR FACTOR (NF)-YB, and NF-YC form a complex that directly activates transcription of *FLOWERING LOCUS T* (*FT*) (Wenkel et al., 2006; Gnesutta et al., 2017). As part of florigen, FT protein moves through the phloem from the distal leaf veins to the shoot apical meristem (SAM) to promote flowering (Corbesier et al., 2007; Tamaki et al., 2007; Turck et al., 2008). *FT* is mainly transcribed in the companion cells (CCs) of the leaf phloem (Kotake et al., 2003; Adrian et al., 2010), which suggests that these cell types alone take responsibility for providing flowering stimuli (Lopez-Salmeron et al., 2019). In contrast, it is still unclear, how many leaf-cell types perceive the photoperiod signal and whether cell-type-specific responses to photoperiod exist. An indication that tissue-specific responses occur was provided by the detection of an independent and robust circadian clock system in the leaf vasculature compared to mesophyll cells after physical separation of leaf tissue (Endo et al., 2014).

Several methods for purifying-specific cell types based on the expression of tissue marker genes have been applied in plants, such as fluorescence-activated cell sorting and isolation of nuclei tagged in specific cell types (INTACT) (Brady et al., 2007; Deal and Henikoff, 2011; Kawakatsu et al., 2016; Svozil et al., 2016). INTACT has been widely used in epigenetic studies due to its low cost and convenient operation (Deal and Henikoff, 2010). In brief, a cell/tissue-specific promoter is chosen to drive an engineered "nuclear targeting fusion" (NTF) protein that is composed of a nuclear envelope localization domain, a GREEN FLUORESCENT PROTEIN, and a biotin receptor peptide. After biotinylation of NTF that is catalyzed by a constitutively expressed bacterial BirA enzyme, nuclei of interest are purified using magnetic streptavidin-coated beads (Deal and Henikoff, 2010, 2011). INTACT has been used to isolate Arabidopsis root hair and nonroot hair nuclei to detect the cell-type-specific gene expression and histone modifications (Deal and Henikoff, 2010) and to explore histone modifications in the SAM and leaf phloem CCs (You et al., 2017, 2019).

We are interested in the specific response of *cis*-regulatory elements in different leaf cells in sensing the LD signal. Two genome-wide methods are available that allow both, detection of accessible chromatin and identification of putative transcription factor binding sites (TFBSs) through the occurrence of protected footprints within accessible chromatin regions (ACRs). While DNase-seq has been adapted to study the regulatory sequences in maize and Arabidopsis (Zhang et al., 2012; Oka et al., 2017; Alvarez et al., 2019; Yan et al., 2019), it is not well suited to be combined with low amounts of starting material. In contrast, assay for transposase-accessible chromatin using sequencing (ATAC-seq), making use of the transposase activity of the Tn5 enzyme coupled with oligonucleotide adapters that allow direct generation of high-throughput sequencing libraries, is well adapted to capture regulatory elements from limited starting material (Buenrostro et al., 2013; Lu et al., 2017; Maher et al., 2018; Potter et al., 2018; Reynoso et al., 2019). In plants, a combination of INTACT and ATAC-seq identified cell-specific ACRs in root hairs, shoot stem cells, and mesophyll cells (Bajic et al., 2018; Sijacic et al., 2018).

Our study investigated cell-type-specific and LD-responsive ACRs and their relative enrichment for TFBS. We separated ACRs with respect to their different genomic location at target genes. We combined INTACT, ATAC-, and RNA-seq to separate single cell types corresponding to phloem CCs and epidermis. In both cell types, chromatin accessibility was generally increased after perception of the LD signal; however, variable and specific response ACR patterns were detected by comparing both cell types. LD-induced ACRs (iACRs) pinpointed previously characterized flowering-related genes but also novel loci, such as *TREHALOSE-PHOSPHATASE/SYNTHASE 9* (*TPS9*), for which we confirmed a positive role in flowering time regulation. iACRs of CCs were particularly enriched for binding events of flowering-related TFs. Our work highlights the importance of cell-type-specific studies to elucidate the function of noncoding elements in the regulation of gene regulatory networks.

Results

INTACT isolation yields highly purified nuclei from Arabidopsis leaf vasculature and epidermis

The leaf is the major organ that perceives photoperiodic signals. Several known floral regulators like *FT* and *CO* are mainly expressed in phloem CC, whereas others like the floral repressors *FLOWERING LOCUS C* (*FLC*) and *SHORT VEGETATIVE PHASE* (*SVP*) do not show a tissue-specific pattern of expression (Kotake et al., 2003; Lee et al., 2007; Castillejo and Pelaz, 2008; Li et al., 2008; Sawa and Kay, 2011). To dissect the specific function of the leaf vasculature in the regulation of flowering, we established an INTACT approach to enrich both phloem and epidermis nuclei.

In the background of Arabidopsis *ACT2p:BirA* expressing transgenic plants (Deal and Henikoff, 2010), we introduced *Cucumis melo GALACTINOL SYNTHASE 1* (*GAS1*) (Haritatos et al., 2000) and Arabidopsis *FIDDLEHEAD* (*FDH*) (Pruitt et al., 2000) promoters to specifically drive the expression of *NTF* in CC and epidermis, respectively (transgenic lines

named *GAS1p:NTF* and *FDHp:NTF*) (Figure 1, A and B). After sorting nuclei according to the INTACT procedure (see Materials and methods section and Deal and Henikoff, 2011), magnetic dynabeads specifically interacted with single nuclei in both *GAS1p:NTF* and *FDHp:NTF* samples, while there were almost no free nuclei in the sorted samples (Figure 1, C and D). To further validate the purity, we introduced a spike-in approach by adding Landsberg *erecta* (L*er*) background material into the *GAS1p:NTF* or *FDHp:NTF* (Col-0 ecotype) samples before sorting (Moreno-Romero et al., 2017), and measured the L*er* to Col-0 DNA ratio before and after INTACT. A purity of >98% was detected for both cell types (Figure 1E).

To understand chromatin accessibility and transcriptome variation in CC and epidermis in response to LD, we performed INTACT sorting after shifting 14-day-old short day (SD) grown seedlings for 3 days to LD; control plants remained in SD until harvest. *GAS1p:NTF* and *FDHp:NTF* plants were sampled before dawn in LD (ZT16) and SD (ZT8) conditions. In our greenhouse conditions, plants shifted for three LD flowered almost as early as plants that were continuously grown in LD (Figure 1F; Supplemental

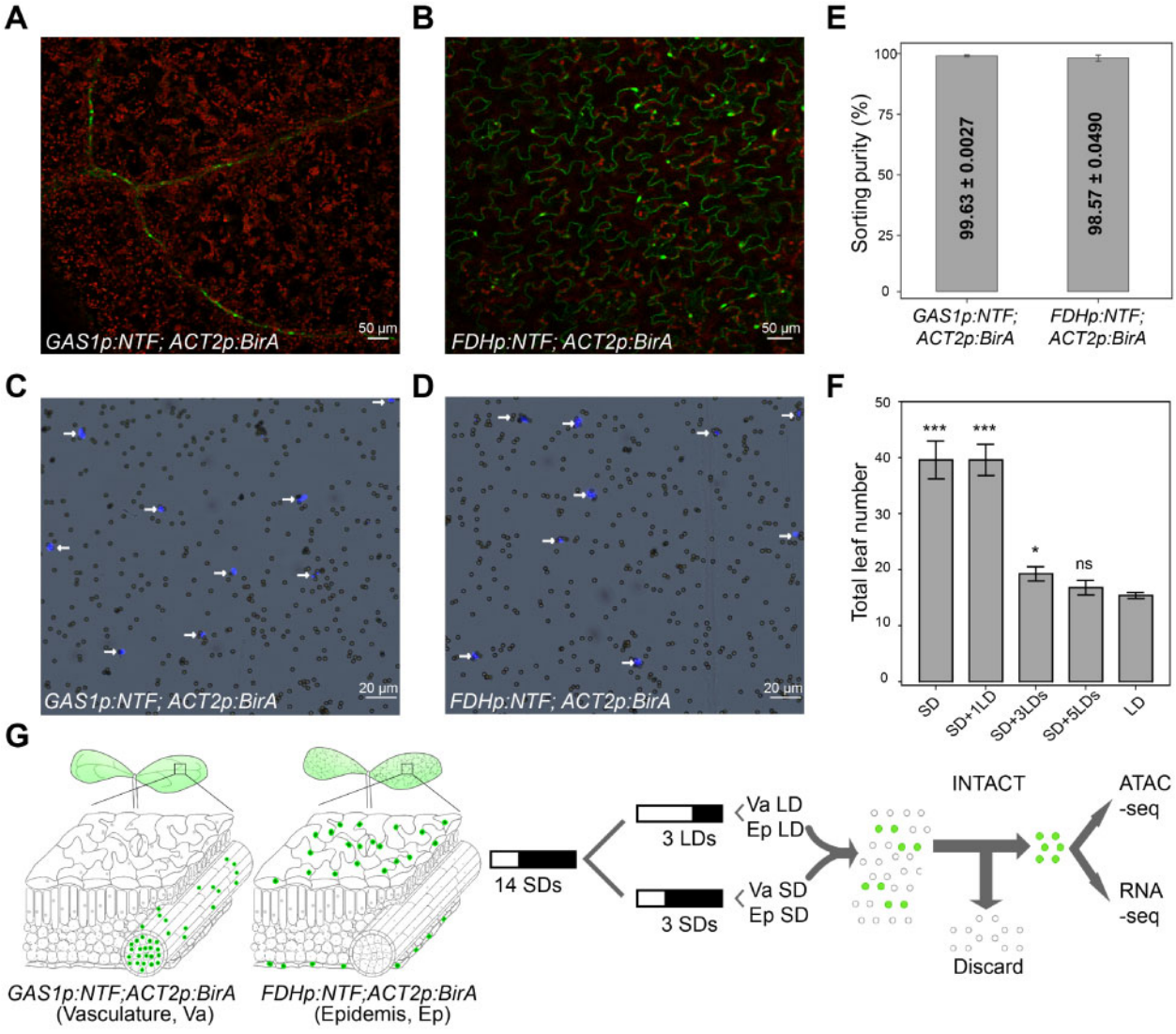

Figure 1 Combination INTACT with ATAC- and RNA-seq to study chromatin accessibilities and gene expressions in vascular and epidermis cells. (A, B) Fluorescence microscopy images showing the cell-type-specific NTF signals (GREEN FLUORESCENT PROTEIN channel) in transgenic plant lines expressing *GAS1p:NTF* (A) and *FDHp:NTF* (B), respectively, in phloem CC and epidermis. Bar = 50 μm. (C, D) Fluorescence microscopy images showing streptavidin-coated magnetic beads after INTACT purification. White arrowheads indicate the beads bound by DAPI-stained NTF-labeled nuclei. Bar = 20 μm. (E) Purity of NTF-labeled nuclei isolated by INTACT from *GAS1p:NTF;ACT2p:BirA* and *FDHp:NTF;ACT2p:BirA* plants detected by comparing relative enrichment of Col-0 and spiked-in L*er* molecular markers before and after purification by qPCR. (F) Flowering time of plants transiently shifted to LD as indicated after 14 days of growth in SD, controls were grown in constant SDs and LDs. Flowering time determined as total leaf number. Bar plots show mean±s.d. Significant differences were determined by *t*-test. $^{*}P < 0.05$, $^{***}P < 0.001$, and ns indicates not significant. (G) Overview of the experimental design.

Figure S1), consistent with previous findings in Arabidopsis (Corbesier et al., 2007). As expected, expression of the flowering integrator gene *FT* was induced after three LD compared to SD controls (Supplemental Figure S2).

Quality control of ATAC-seq data and identification of ACRs

INTACT-isolated nuclei from leaf vascular CC (Va LD and Va SD) and epidermis cells (Ep LD and Ep SD) were further analyzed for their transcriptome and chromatin accessibility (Figure 1G; Supplemental Table S1). To evaluate the quality of our ATAC-seq data, we compared it with published DNase-seq (Zhang et al., 2012) and ATAC-seq (Lu et al., 2017; Maher et al., 2018; Potter et al., 2018) datasets. After removing organellar reads from the total filtered reads, on average 88% (ranging from 84% to 93%) nuclear genomic reads remained in our data set, which is comparable to the genomic reads in published data (Supplemental Figure S3). To identify ACRs, the enrichment of ATAC-seq reads was analyzed by using MACS2 (Model-based Analysis of ChIP-Seq 2) peak mapping software (Zhang et al., 2008b). Overlapped peaks called in both biological replicates of each cell type and treatment were considered as ACRs. We identified 16,847, 19,501, 15,064, and 17,330 ACRs in Va LD, Ep LD, Va SD, and Ep SD, respectively (Supplemental Figure S4A). Compared to published data, >80% of DNase I Hypersensitive Sites from wild-type leaves (Zhang et al., 2012) were reproduced in our INTACT-ATAC ACRs (Supplemental Figure S4B).

To estimate the signal to noise ratio of our ATAC-seq data, we analyzed the Signal Portion of Tags (SPOTs) value, which counts the percentage of nuclear reads enriched at ACRs compared to all mapped reads. We found average SPOT values ranging from 68% to 79%, which is comparable to SPOT average values of published data (Supplemental Figure S5). A genome browser overview of an exemplary 200-kb genomic region illustrates the occurrence of enriched signals as sharp peaks and a comparable low background in all four samples (Figure 2A). We performed a principal component analysis (PCA) comparing the enrichment values at all ACRs across all samples. Biological replicates clustered most closely together (Supplemental Figure S6). Taken together, 15,000–20,000 ACRs were identified in each leaf cell type grown in different photoperiods from a dataset of high quality.

Differential features of proximal and distal ACRs

We further analyzed the distribution of ACRs to different genomic regions in all four samples. The majority of ACRs (~86%) localized at gene proximal regions [including <1-kb upstream of the transcriptional start site (TSS) ~53%, genebody ~22%, and <1-kb downstream of the transcription termination site (TES) ~11%] and a minority (~14%) of ACRs at gene distal or intergenic regions (Figure 2B). When overlapped with a previously determined set of conserved non-coding sequences (CNSs) (Van de Velde et al., 2014), the intergenic ACRs enriched a higher fraction of CNS than proximal ACRs and control regions (Figure 2C). Enrichment of putative Arabidopsis TFBS, which were determined using available DAP-seq peaks for 529 TFs (O'Malley et al., 2016) was detected for proximal and distal ACRs over control regions (Figure 2D). In addition, the expression level of genes associated only with TSS or genebody ACRs was significantly higher than those only with intergenic or TES ACRs, while genes associated with more than one ACR category expressed overall at higher levels than those associated with fewer (Figure 2E).

Taken together, ACRs overrepresented CNS and putative TFBS, the presence of a proximal and/or genebody ACRs correlated with higher expression of associated genes than their absence and a general additive trend of ACRs of different categories on gene expression levels became obvious.

The chromatin response to day length is tissue-specific

To further understand variation in chromatin accessibility during the shift from SD to LD in leaf-vasculature CC and epidermis cells, we identified responsive ACRs that were differentially enriched between samples (Supplemental Figure S7A and see Materials and methods section). If an ACR was identified in both biological replicates with MACS2 (FDR [false discovery rate] < 0.01) and showed increased or decreased tagment signals >1.5-fold after the shift from SD to LD in vasculature, it was considered as vasculature induced and repressed ACRs (i/rACRs); the same criteria were applied to identify epidermis i/rACRs (Supplemental Figure S7A and see Materials and methods section). Cell-type-specific responsive ACRs were further classified as vasculature-specific (Va), epidermis-specific (Ep), and overlapped (Va&Ep) i/rACRs (Supplemental Figure S7, B and C and Materials and methods section).

Overall, we obtained 6,196 iACRs, composed of 2,861 Va iACRs and 1,486 Ep iACRs as well as 1,849 Va&Ep iACRs (Figure 3A; Supplemental Figures S7 and S8; Supplemental Data Set 1). In general, LD predominantly leads to chromatin opening and phloem CCs appear to be more sensitive than cells of the epidermis, since the number of Va iACRs was ~2 times higher than that of Ep iACRs. Overall, the number of rACRs was dramatically smaller than that of iACRs; 185 rACRs were counted as Va-specific, 722 as Ep-specific, and 138 as overlapping between the tissues (Figure 3B; Supplemental Figures S7 and S8; Supplemental Data Set 1). Most responsive ACRs showed quantitative changes of chromatin accessibility; however, in rare cases, ACRs were unique to a specific photoperiod condition (Supplemental Figure S9).

Genes associated with iACRs enriched several gene ontologies (Figure 3C; Supplemental Data Set 2). Importantly, large differences in enriched GO-terms were found between vasculature and epidermis cell types. Pathways related to circadian rhythm, regulation of gene expression, developmental processes, and hormone response enriched predominantly in the vasculature CC, whereas pathways related to defense

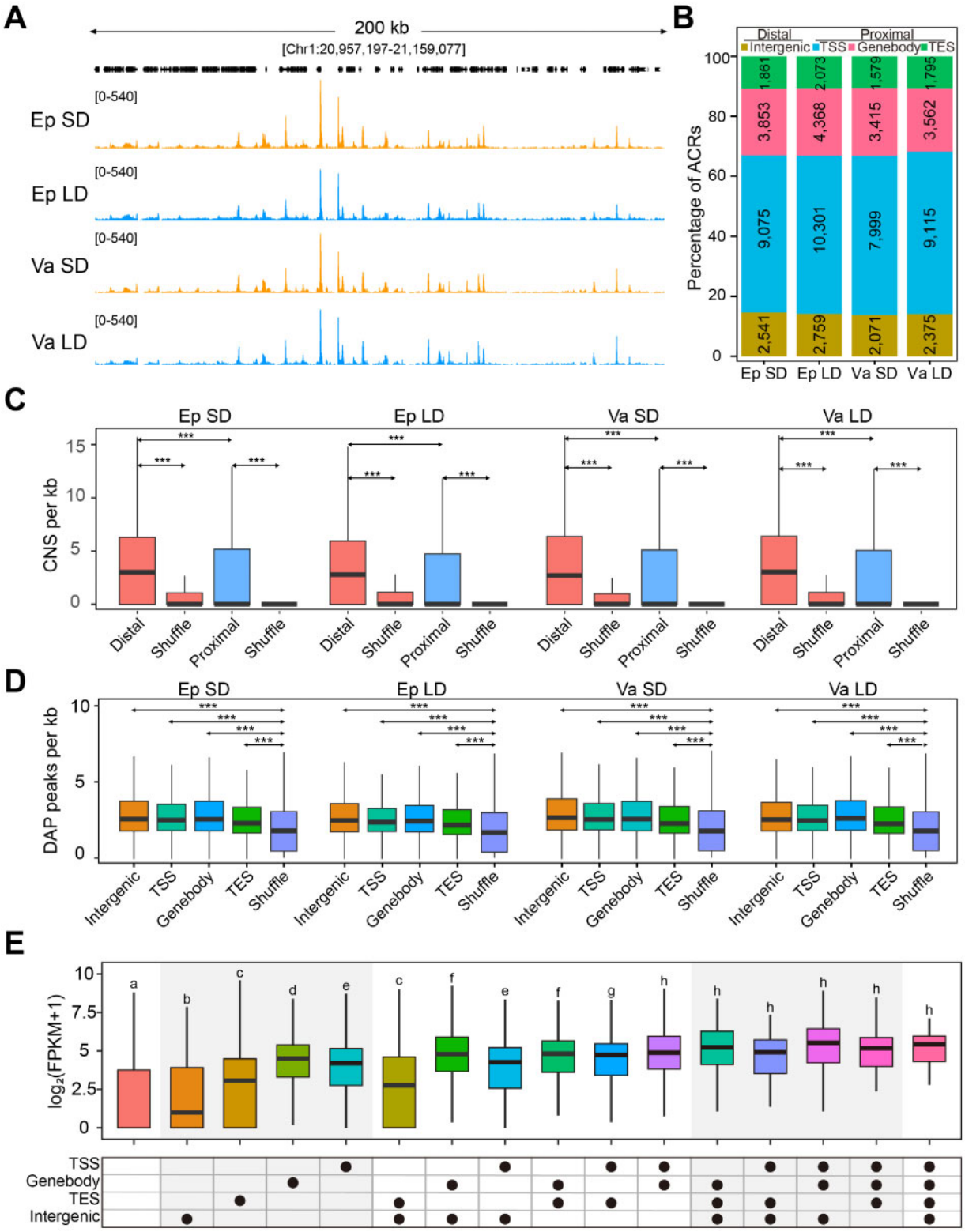

Figure 2 Characterization of the proximal and distal ACRs. (A) Genome browser showing ATAC-seq signals in a 200-kb region (Chr1:20,957,197-21,159,077) in four samples as indicated. Tracks show normalized values of one representative biological replicate for each sample. (B) The percentage of ACRs corresponding to categories Intergenic, TSS, Genebody, and TES for Ep SD, Ep LD, Va SD, and Va LD. TSS: ACRs located within −1,000 to +50 bp of a gene's TSS; TES: ACRs located within −50 to +1,000 bp of a gene's TES; Genebody: ACRs located within the genebody; Intergenic: all other ACRs. Number of ACRs indicated in bar plots. (C) Enrichment of conserved CNSs in distal (Intergenic) and proximal (all other ACRs) regions, control shows shuffled sequences from all ACRs. *P*-values were calculated based on Wilcoxon signed-rank tests. $^{**}P < 0.01$. (D) Boxplots showing the number of potential TFBS in different ACR categories. 529 DAP-seq derived matrices for TFs were included in the analysis. *P*-values were calculated based on Wilcoxon signed-rank tests. $^{***}P < 0.001$. (E) Boxplots showing expression levels of genes associated with TSS, Genebody, TES, and Intergenic ACRs. Boxplots show the median (horizontal line), second to third quartiles (box), and Tukey-style whiskers (beyond the box). Statistical significance was calculated based on pairwise Wilcoxon signed-rank tests.

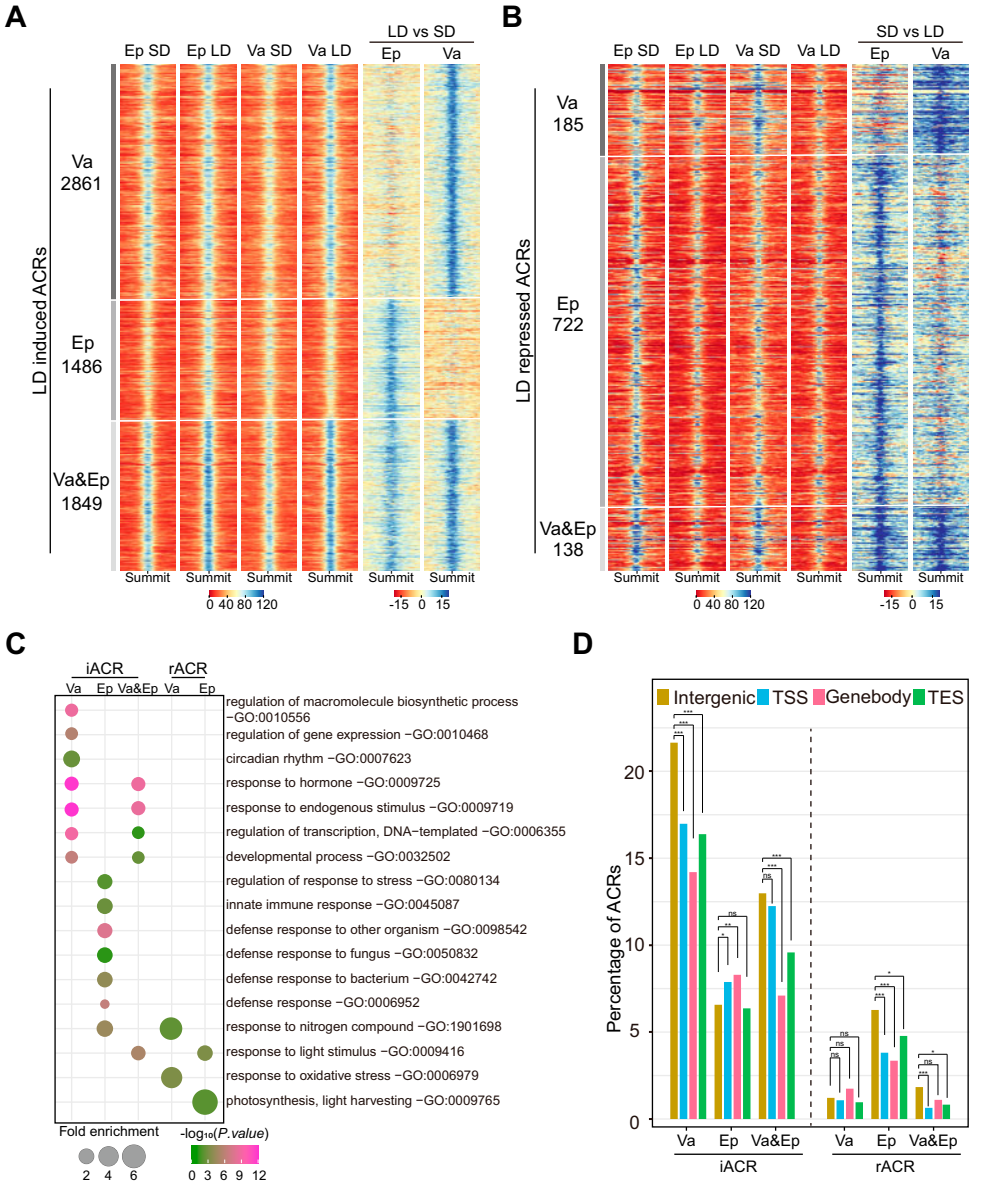

Figure 3 Characterization of LD induced or repressed ACRs in isolated cell types. (A) and (B) Heatmaps showing ATAC-seq coverage from −1 to + 1 kb around the center of LD-induced (A) and LD-repressed ACRs (B). Right panels show fold-changes in coverage between SD and LD samples. Va response ACRs; Ep response ACRs; Va&Ep, overlapped response ACRs between two tissues. (C) GO analysis showing enriched pathways of genes associated with LD-induced and LD-repressed ACRs per cell-type-specific category. (D) Bar plots showing percentage of responsive ACRs per ACR category. The number of all ACRs per category and tissue type is set to 100%. *P*-values were calculated based on Fisher's exact tests. $^{*}P < 0.05$, $^{**}P < 0.01$, $^{***}P < 0.001$, and ns indicates not significant.

response, stress response, and response to bacteria and fungi enriched in epidermis cells (Figure 3C). Genes associated with rACRs in the vasculature CC enriched GO-terms related to response to nitrogen compounds and oxidative stress, while rACR associated genes in epidermis cells enriched pathways related to photosynthesis, light harvesting, and light stimulus (Figure 3C). We evaluated if ACRs corresponding to different genomic categories showed a different response to photoperiod changes and whether such differences were tissue specific. A comparison of the fraction of responsive ACRs within each genomic category showed that distal iACRs were the most responsive category in the Va samples while a slightly higher proportion of proximal (TSS and genebody) ACRs were induced by LD in the epidermis (Figure 3D; Supplemental Figure S10).

Taken together, chromatin regions are more likely to open than close during a shift to LD in both leaf cell types and this trend is even stronger in vasculature CC than that in epidermis cells. In CC, the proportion of distal ACRs induced by LD is higher than that of proximal ACRs, while a trend

toward induction of proximal ACRs is detected in the epidermis. Despite a large overlap in the response, distinct gene sets respond predominantly to the change in photoperiod in epidermis and vasculature.

Altered chromatin access at distal and proximal ACRs correlates with gene expression

Gene expression is strongly correlated with chromatin accessibility at TSS (Sullivan et al., 2014; Klemm et al., 2019), but a similar link could so far not be established between gene expression and distal ACRs in plants (Oka et al., 2017). INTACT-sorted nuclear RNA-seq has been widely used to analyze global gene expression in root hair, nonroot hair, mesophyll, phloem, and shoot meristem cells (Deal and Henikoff, 2010; You et al., 2017; Sijacic et al., 2018; You et al., 2019). It was previously shown for plants and animals that nuclear RNA-seq data can represent similar expression profiles as whole-cell RNA-seq data (Jacob et al., 2007; Zhang et al., 2008a). To evaluate how photoperiod-induced differential gene expression was related to proximal and distal ACRs in leaf vasculature and epidermis, we carried out RNA-seq with INTACT isolated nuclei (see Materials and methods section).

Pairwise comparisons were performed among the four samples; genes with greater than two-fold change and FDR < 0.05 were considered as differentially expressed genes (DEG). Generally, more vascular genes were activated in LD, whereas more epidermis genes were repressed. Among the LD-activated DEG, 408 were specific to the vasculature, 257 to the epidermis, and 288 detected in both cell types. Among the LD-repressed DEG, 145 were specific to the vasculature, 507 to the epidermis, and 330 detected in both cell types (Figure 4A; Supplemental Data Set 3). Tissue-specific marker genes such as *ALTERED PHLOEM DEVELOPMENT* (Bonke et al., 2003) and *ARABIDOPSIS THALIANA ARABIDOPSIS H(+)-ATPASE 3* (DeWitt and Sussman, 1995) for vasculature, as well as *ECERIFERUM 1* (Bourdenx et al., 2011) and *PERMEABLE LEAVES 3* (Panikashvili et al., 2009) for epidermis were detected as differentially expressed in our RNA-seq dataset (Supplemental Figure S11A). GO-term enrichment analysis revealed that DEG in the vasculature CC related to hormone response and endogenous stimulus, and to pathways related to defense response and light stimulus in epidermis cells (Supplemental Figure S11B).

Gene expression in LD clearly increased with increasing chromatin accessibility; likewise, reduced expression was linked to decreased chromatin access as roughly 70% of all dynamically changing proximal and distal ACRs showed a correlated variation in the expression of associated genes (Figure 4B). To test the significance of the observed relationship between differential chromatin accessibility and gene expression, we created random permutations of the DEG dataset and re-calculated how DEG related to i/rACRs after permutation. Across both tissues and irrespective of the genomic location of ACRs, the number of upregulated DEG related to iACRs and that of downregulated DEG related to rACRs was significantly higher than expected (Figure 4C). Representative examples for LD responsive i/rACRs associated with DEGs in vasculature CC and epidermis are shown in a genome browser (Figure 4D).

In sum, changes in chromatin access can be directly linked to gene expression not only for proximal but also for distal intergenic ACRs. Cell types carry a significant chromatin-to-expression-change signature, which may be linked to their selective response to the LD signal.

Identification of flowering regulators in the phloem based on chromatin-to-expression signature

We ranked our data sets according to the occurrence of distal and proximal iACRs related to transcriptional induction. Among the 14 top-ranked genes from the leaf CC dataset (Supplemental Data Set 4), genes with an established or putative link to flowering were prominent: *ARABIDOPSIS RESPONSE REGULATORS* (*ARRs*) *7*, *ARR4*, and *BBX17* clustered to the proximal ACR group; and *FT* and *TPS9* clustered to distal ACR group (Figure 4E; Supplemental Figure S12).

We previously identified a distal enhancer, *Block C*, which participates in promoting *FT* expression in the leaf vasculature under LD (Adrian et al., 2010; Liu et al., 2014). The chromatin accessibility in the *Block C* region increases in response to LD, particularly in CCs, a result that could be confirmed by an independent ATAC-qPCR (ATAC followed by quantitative real-time PCR) assay (Figure 5A). As expected, RNA-seq data show that *FT* expression was significantly induced by LD in CC (Figure 5A). These results demonstrate that a characterized distal enhancer of *FT* carries the typical chromatin-to-expression signature that is observed in genome-wide data.

We selected *TPS9* as a new representative for an analysis of gene function, which shows rapidly changing expression levels according to a light/dark diurnal cycle (Usadel et al., 2008). TPS1, a homolog of TPS9, accelerates the floral transition by both, activating *FT* expression in leaves and promoting the flowering program in SAM (Wahl et al., 2013). The promoter of *TPS9* drives expression of the *GUS* reporter gene in the vasculature of leaves, roots, and shoot apices (Ramon et al., 2009); however, the biological function of *TPS9* is not yet resolved.

Chromatin accessibility of ACR associated with *TPS9* gene as well as RNA abundance was obviously higher in Va LD compared to Va SD (Figure 5B). In detail, we found 1.7-fold change (Va LD/Va SD) at iACR2 associated with the promoter of *TPS9* (Figure 5B). ATAC-seq results were confirmed by ATAC-qPCR using primers to measure the relative fold changes at iACR2 of *TPS9* (Figure 5B). To assess a potential function of *TPS9* in the floral transition, we characterized Salk T-DNA insertion mutants. Two independent *tps9* mutant lines (SALK_086992C and SALK_151275C, named *tps9-1* and *tps9-2*, respectively) flowered significantly later than Col-0 control in LDs (Figure 5C; Supplemental Figure S13), while no obvious difference of flowering time was observed in SDs (Supplemental Figure S14) indicating that *TPS9*

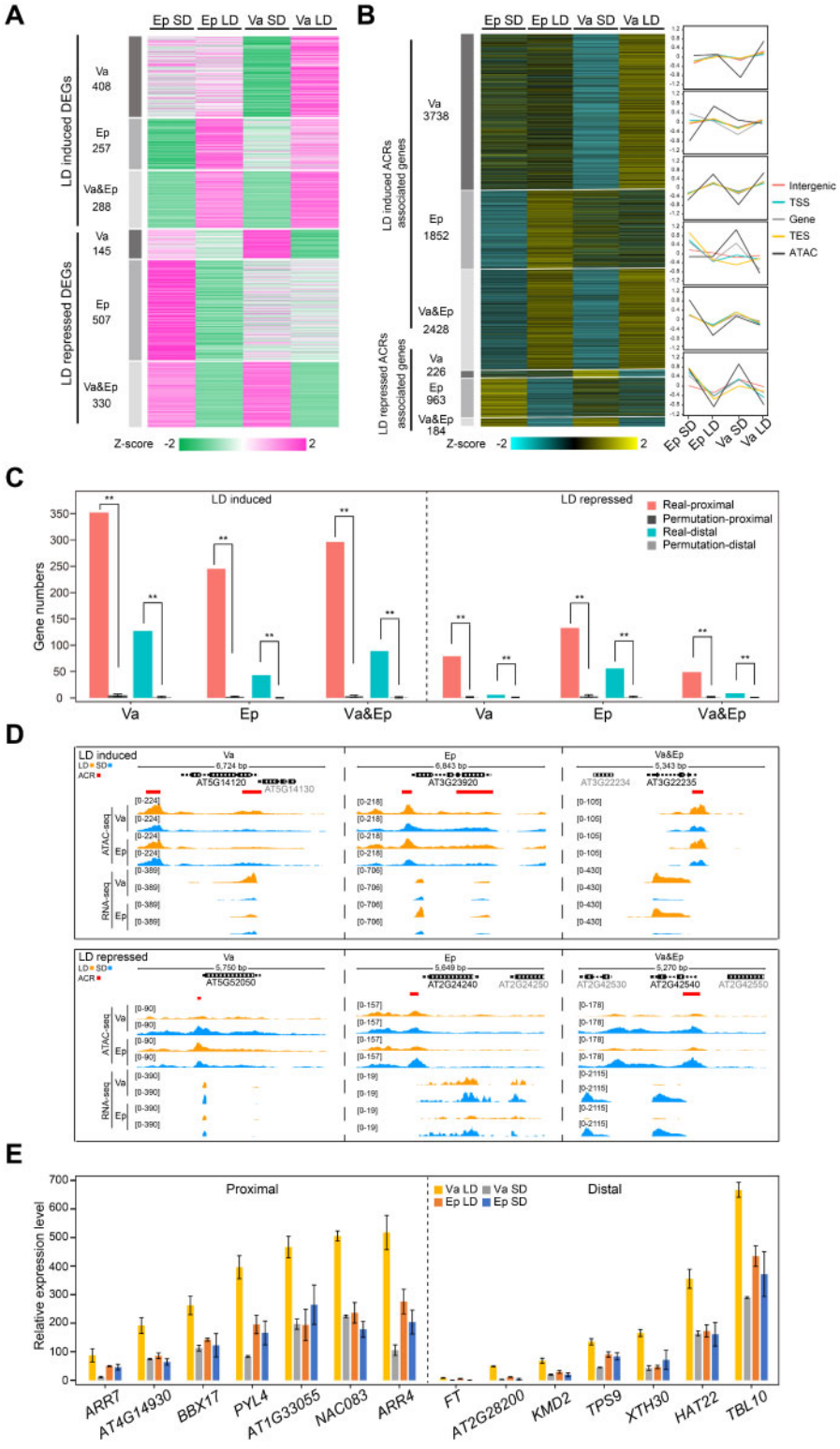

Figure 4 Chromatin accessibility variation is correlated with differential gene expression. (A) Heatmap showing the Z-score of expression for each gene grouped by different DEG category. (B) Heatmap and average line plots showing Z-scores of expression variation for each gene associated with different ACR categories. For each tissue response type, the right panel shows the relative level of chromosome accessibility enrichment (black) and averages of gene expression scores per ACR categories: Intergenic (red), TSS (blue), Genebody (gray), and TES (yellow). (C) Association of responsive ACR categories [distal (Intergenic) and proximal (all other categories) per tissue type] with genes that show correlated differential expressed. Significant *P*-values were calculated with a permutation test ($n = 100$). $^{**}P < 0.01$. (D) Genome browser showing ATAC-seq and RNA-seq signals around representative LD activated or repressed ACRs in vascular and epidermal cells. Note that changes in expression level of associated genes change in the same direction as chromatin access at ACRs. (E) Representative candidates of LD activated DEGs in phloem CCs that are associated with proximal (left panel) or distal iACRs (right panel). Raw read counts were normalized with DEseq2 for each tissue and treatment to compare gene expression in different samples.

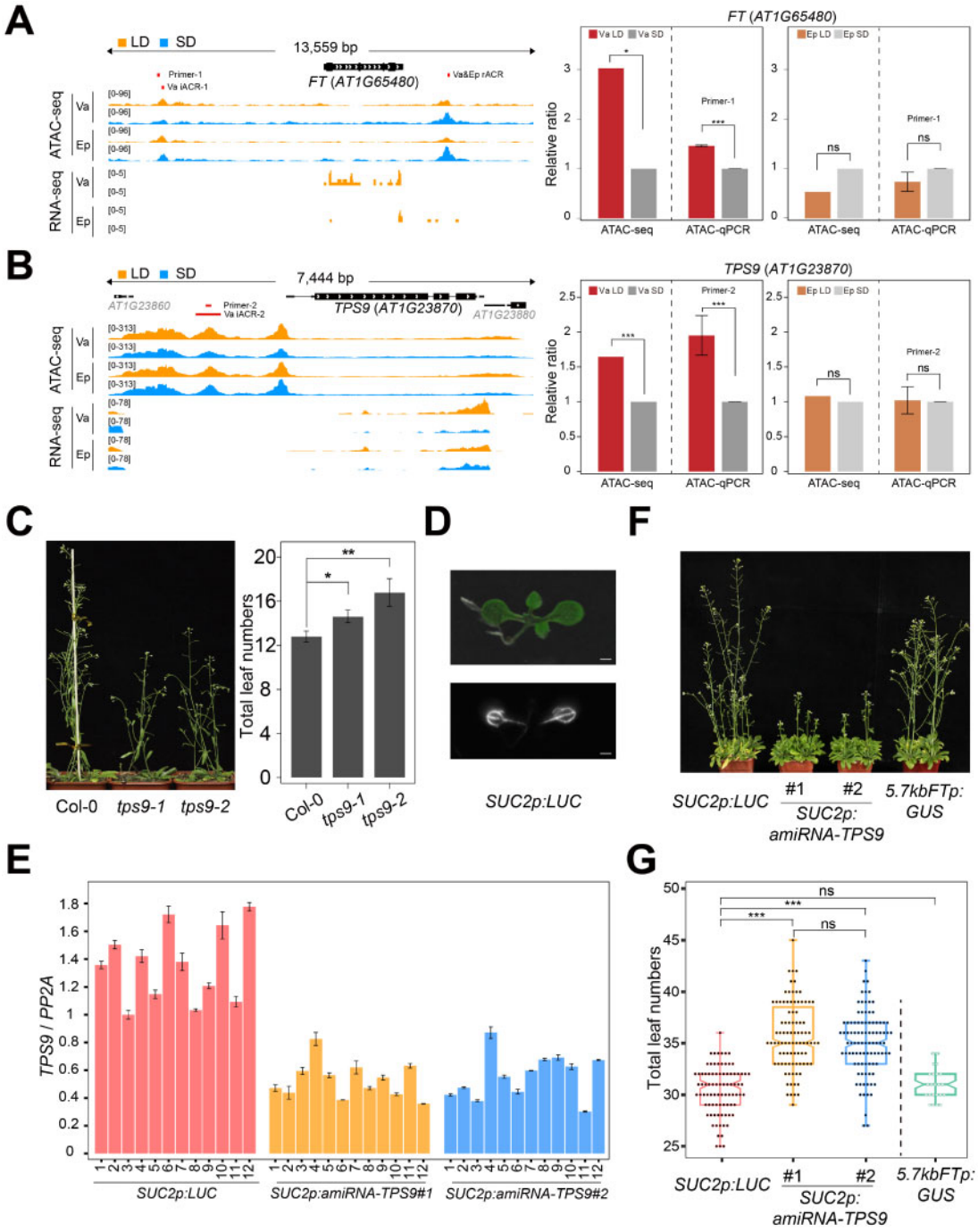

Figure 5 *FT* and *TPS9* associated with LD induced ACRs promote floral transition. (A and B) Genome browser tracks showing ATAC- and RNA-seq coverage around *FT* and *TPS9* in vascular and epidermis cells. Orange and blue colors mark the LD and SD treatments, respectively. ACRs and primers are indicated as red boxes. Relative density of ATAC-seq signals and ATAC-qPCR enrichment for *FT* and *TPS9* genes are shown in the panels on the right. For ATAC-qPCR, bar plots show mean±s.d. based on two biological replicates, and each biological replicate we included three PCR technical replicates. ATAC-seq *P*-value was calculated by Poisson test. $^{*}P < 0.05$, $^{***}P < 0.001$, NS indicates not significant. ATAC-qPCR *P*-value was calculated by *t* test. $^{***}P < 0.001$, ns indicates not significant. (C) Representative image and flowering phenotype of wild-type Col-0, *tps9-1*, and *tps9-2* plants. Bar plots show mean±s.d. of total leaf numbers in wild-type Col-0 (n = 18), *tps9-1* (n = 21), *tps9-2* (n = 17). *P*-value was calculated by *t*-test. $^{*}P < 0.05$ and $^{**}P < 0.01$. (D) Bioluminescent image of transgenic plant *SUC2p:LUC*. Bar = 100 μm. (E) *TPS9* expression levels were measured by RT-qPCR in 12 independent transgenic lines of *SUC2p:LUC*, *SUC2p:amiRNA-TPS9#1*, and *SUC2p:amiRNA-TPS9#2*. Two mature leaves were collected from one transgenic plant harboring 7–8 true leaves. *PP2A* was used as internal control. Bar plots show mean±s.d. of three technical replicates. (F) The flowering-time phenotype of *SUC2p:amiRNA-TPS9* and two controls of *SUC2p:LUC* and *5.7kbFTp:GUS*. Basta positive plants were transferred to new soil pots in SDs for 3 weeks, and then shifted to LDs until bolting. The transgenic plants of *SUC2p:LUC* treated as vector control; and *5.7kbFTp:GUS* in Col-0 background were treated as Basta positive control. Image of representative plants per genotype. (G) Number of total leaves in *SUC2p:LUC* (n = 86 independent T1 lines), *SUC2p:amiRNA-TPS9#1* (n = 91 independent T1 lines), *SUC2p:amiRNA-TPS9#2* (n = 95 independent T1 lines) and *5.7kbFTp:GUS* (1 homozygous line, n = 23 individuals). Boxplots show the median (horizontal line), second to third quartiles (box) and s.d. (beyond the box). *P*-value was calculated by *t* test. $^{***}P < 0.001$, ns indicates not significant.

contributes to promoting the floral transition in a photoperiod-dependent manner.

To further access the function of phloem-expressed *TPS9* in flowering time regulation, we generated transgenic lines that knock-down *TPS9* specifically in the phloem. Two independent artificial microRNAs (amiRNA), *amiRNA-TPS9#1* and *amiRNA-TPS9#2*, which target exons 2 and 3 of *TPS9*, were driven by the phloem-specific *SUCROSE-PROTON SYMPORTER 2* (*SUC2*) promoter (Truernit and Sauer, 1995) in the Col-0 background (Supplemental Figure S13). As control, a *SUC2p:LUC* (*Luciferase* gene) transgenic line showing a significant signal in leaf veins was used (Figure 5D). In addition, to remove the side effect on plant development by the herbicide Basta (glufosinate) that was used for selection of transgenic plants (Abdeen and Miki, 2009; Christ et al., 2017), we included the Basta-resistant homozygous line *5.7kbFTp:GUS*/Col-0 (Adrian et al., 2010) as control. The expression levels of *TPS9* were significantly lower in *SUC2p:amiRNA-TPS9* than in *SUC2p:LUC* leaves (Figure 5E), while no significant expression difference between the genotypes was detected in shoot apices (Supplemental Figure S15). Like the *tps9* T-DNA insertion mutants, *SUC2p:amiRNA-TPS9* plants flowered significantly later than both control lines (Figure 5F). For statistical analysis of flowering time, we measured around 90 independent transgenic T1 lines for each vector, and found that there were about five more leaves in *SUC2p:amiRNA-TPS9*#1 and #2 lines compared to *SUC2p:LUC* controls (Figure 5G).

A signature of iACR and up-regulated expression in response to LD in leaf phloem CCs taken together, revealed a critical and tissue-specific role of *TPS9* in the timing of flowering.

Transcription factor binding sites of floral regulators are enriched in vascular induced ACRs

The observed predominant increase of chromatin accessibility in response to LD (Figure 3), suggests that transcription factors (TFs) may be recruited to iACRs in LD (Jiang, 2015). We extracted flowering-related TFs from 306 flowering time genes that were collected in the Flowering-Interactive Database (FLOR-ID) (Bouche et al., 2016)), leading to the selection of 10 TF with available ChIP-seq and/or DAP-seq data. Included were six available ChIP-seq (*PHYTOCHROME-INTERACTING FACTOR 4* [*PIF4*], *SUPPRESSOR OF OVEREXPRESSION OF CO 1* [*SOC1*], *FLOWERING LOCUS M* [*FLM*], *iFLMβ*, *FLC*, and SVP) and six DAP-seq (*AGAMOUS-LIKE 15* [*AGL15*], *LATE ELONGATED HYPOCOTYL* [*LHY*], *CDF3*, *VERNALIZATION1* [*VRN1*], *SQUAMOSA PROMOTER BINDING PROTEIN-LIKE 5* [*SPL5*], and *SVP*) data sets (Kaufmann et al., 2010; Deng et al., 2011; Immink et al., 2012; Pose et al., 2013; Pfeiffer et al., 2014; Mateos et al., 2015; O'Malley et al., 2016; Collani et al., 2019). We found enrichment for most potential (determined by DAP-seq analysis) and active TF-binding events (determined by ChIP-seq) at iACRs with slightly higher significance scores in categories that included vascular samples. In contrast, TF-binding events were more significantly enriched at rACRs that included Ep tissues (Figure 6A).

To further test this overall trend, binding for all flowering-related TFs per ACR was normalized to length in kb and compared to regions of the same size randomly sampled from the Arabidopsis genome. Again, flowering-related TFs enriched preferentially at Va iACRs and Va&Ep iACRs compared to Ep iACR while more enrichment was detected at rACRs that did exclude the Va-specific category (Figure 6B). To evaluate to which extent the observed trend was related to the flowering-related bias in the selection of TFs, we analyzed all available DAP-seq data. Enrichment at responsive ACRs was detected for six TF families (TCP [TEOSINTE BRANCHED1/CYCLOIDEA/PROLIFERATING CELL FACTOR], MYB [myeloblastosis]-related, Homeobox/HB, FAR1 [FAR-RED IMPAIRED RESPONSE1], and CAMTA [calmodulin binding transcription activator]) mostly confirming the trend observed for flowering-related factors, with the notable exception of the CAMTA family, which showed the strongest enrichment for rACRs that included vascular samples and a slight preference for iACRs that included epidermis (Supplemental Figure S16; Supplemental Data Set 5).

To build cell-type-specific floral TF regulatory networks related to photoperiod change and flowering time regulation, we build a graphical map of interactions that included 6 flowering-related TFs and 16 flowering genes from the 306 FLOR-ID database that were associated with LD-responsive ACRs of different categories (Figure 6C). We also included *TPS9* in the networks based on our validation of its phloem-specific role in flowering time regulation in LD. As expected from the previous analysis, a higher proportion of genes was connected to Va and Va&Ep iACRs than Ep iACRs, since only 2 out of 17 genes showed Ep-specific connectivity. Only three associations between flowering-related TFs and rACRs occurred (Figure 6C). LHY as a component of the circadian clock is connected to *TPS9* through a Va iACRs located at the TSS. At *FT*, a LHY TFBS locates within the enhancer *Block E* located downstream of the gene, a second LHY-binding site is located with the distal enhancer *Block C*, which overlaps with an iACR (Figure 6, C and D). It should be noted that interactions between flowering TFs and flowering-related DEG were not restricted to ACRs or open chromatin regions, that is, CDF3, SVP, FLC, and VRN1 association outside of these regions was detected for *FT* and *TPS9* (Figure 6D).

We also attempted to construct TF gene regulatory networks based on DEG. For flowering-related TFs, enrichment of binding sites was only informative to predict differential expression, if gene-associated ACRs were located at the TSS (Supplemental Figure S17). On the other hand, a tissue-specific network topology was clearly detected when the iACRs were connected to all available DAP-seq TF that was associated to DEG (Supplemental Figure S18). The topology suggests a clear separation of active gene regulatory modules acting in phloem CC and epidermis that does not

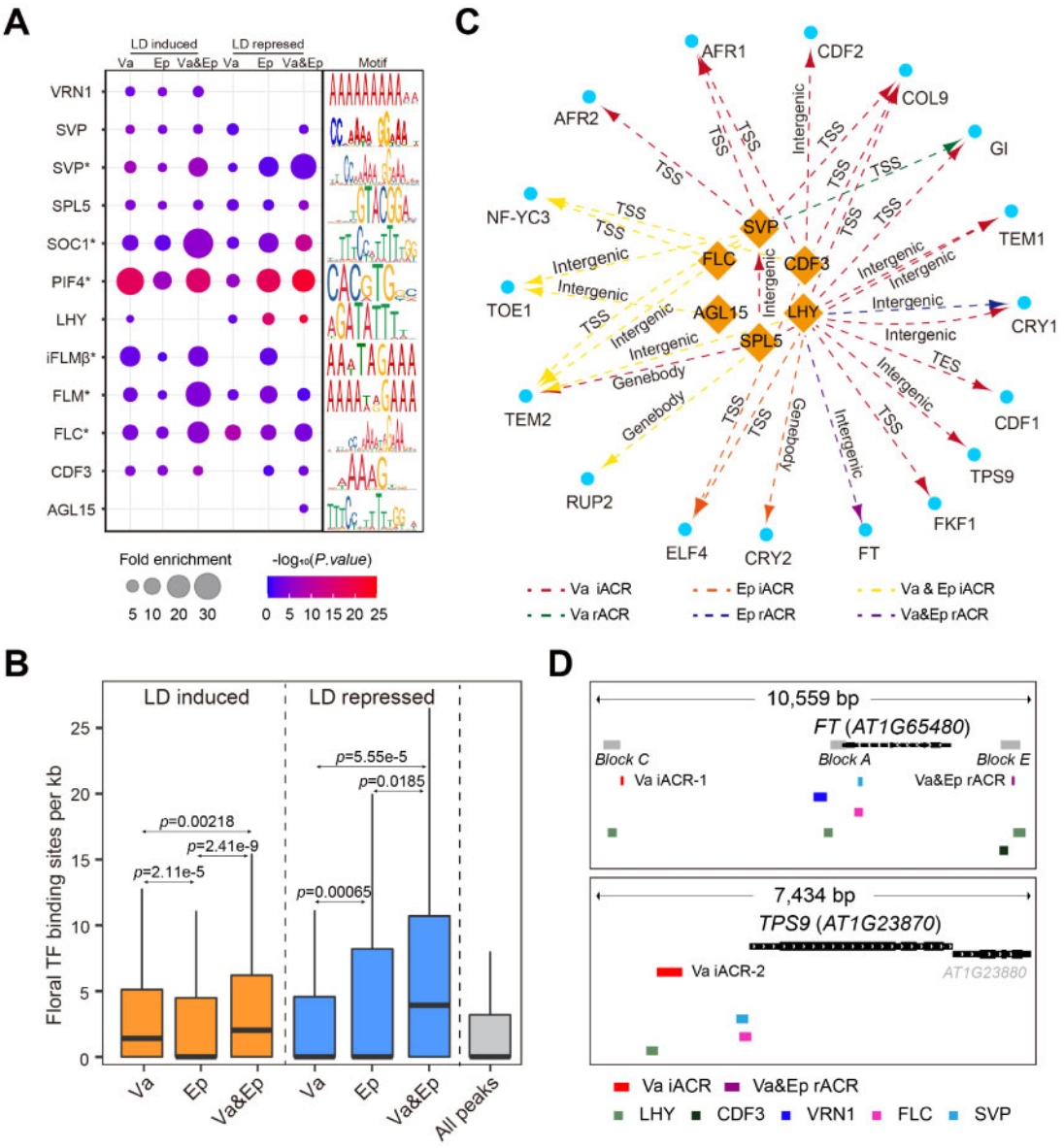

Figure 6 Floral TFs are enriched to regulatory ACRs in LD vasculature. (A) Bubble plots showing enrichment of flowering-related TFs at genes associated with LD induced and LD repressed ACRs. Six ChIP-seq datasets (marked by asterisk) and 6 DAP-seq for 10 floral regulators was included in the analysis. (B) Boxplots showing the number of binding sites of 10 flowering-related TFs at associated ACRs. Boxplots show the median (horizontal line), second to third quartiles (box), and Tukey-style whiskers (beyond the box). *P*-values were calculated based on Wilcoxon signed-rank tests. (C) Network showing binding interactions of six flowering-related TFs (rhombus) with i/rACR regions of associated with genes that are related to flowering (circle). (D) Genome browser tracks showing ATAC-seq coverage and binding sites of flowering-related TFs for *FT* and *TPS9*. Va iACRs were marked by red boxes. *Blocks A*, *C*, and *E* were marked by grey boxes at *FT* locus.

predominantly involve TF and genes with a confirmed role in flowering time regulation.

Taken together, our results indicate that flowering-related TFs predominantly associate with LD-induced ACRs especially in samples that include phloem CCs, while they are more associated with rACRs in the epidermis. This trend is not restricted to TF not currently associated with a role in flowering time regulation, although the CAMTA TF family followed an opposite trend. Overall, for flowering-related TFs, differential gene expression was less informative than differential ACRs, unless these were located at the TSS.

Discussion

Cell-type-specific responsive ACRs during photoperiod change identified by INTACT-ATAC

Transcriptional regulation and changes in chromatin states are functionally interconnected, but the causality of their interactions is not yet fully understood. In this study, we focused on dissecting how plants differentially sense and translate a change in the day-length signal in two leaf tissues. We isolated vasculature CC and epidermis nuclei from leaves and analyzed chromatin accessibility and

transcriptomes in response to LD. We observed a predominant increase in chromatin accessibility upon a change to LD photoperiod that was shared between cell types, but we also detected cell-specific dynamics, indicating that both cell types sense the change in photoperiod and that they engage different gene networks in their response to the signal (Figures 2 and 3).

Phloem CCs are specialized living cells in the leaf vasculature playing functions in ion transport, sugar translocation, and inter-organ communication including the photoperiodic response (Lopez-Salmeron et al., 2019). Several floral activators such as *CO*, *FT*, and repressors like *TEM1* mainly express in phloem CCs (Castillejo and Pelaz, 2008; Turck et al., 2008; Adrian et al., 2010). Not unexpectedly, CC-specific changes in chromatin accessibility and associated changes in transcription affected genes involved in the regulation of flowering. In contrast, Ep responses were either related to biotic and abiotic stress or photosynthesis genes, for ACRs with, respectively, increased or decreased ATAC-seq signal. Interestingly, the location of responsive chromatin regions was distinct for both cell types: In CCs, an increase in chromatin accessibility is more likely to occur in gene-distal as in gene-proximal regions, while an increase is more often gene-proximal in the epidermis. These differences could be driven by the nature of the affected gene regulatory networks, their overall expression level, or other chromatin features. Indeed, it was recently shown that active and repressive histone marks H3K27me3 and H3K4me3 were mutually antagonistic in phloem cells during a response to photoperiodic change (You et al., 2019). Thus, there may be an extended correlation between the occurrence of distal ACRs and the prevalence of Polycomb Group and Trithorax Group-related epigenetic marks.

Open chromatin regions are preferred sites of active TF binding; in reverse, active transcription factor binding is likely to increase chromatin accessibility; furthermore, increased transcription per se may lead to open chromatin, in particular at proximal ACRs (Klemm et al., 2019). In our study, we found that many iACRs in CCs were bound by TFs related to flowering, based on the re-analysis of ChIP-seq datasets, or at least likely to contain flowering-related TFBS based on available DAP-seq data (Figure 6). This observation suggests that the increase in chromatin accessibility could be a consequence of the induction of flowering related TFs upon LD perception; however, it is also possible that single TFs in this group are responsible for a synchronized opening of ACRs at these genes, promoting the binding of other TFs. A previous study suggested that the binding of AP1 (APETALA1) and SEP3 (SEPALLATA3) MADS-box TFs precedes an increase in chromatin accessibility at their target regions during floral development (Pajoro et al., 2014). In the future, it will be interesting to differentiate between cause and consequence in the relationship between TF binding and chromatin access.

Cell-type-specific photoperiod responsive gene regulatory networks

To further investigate cell-type-specific interactions of TF and ACRs, we compared the association of TF families with cell-type-specific ACRs showing increased or decreased accessibility in response to LD using publicly available DAP-seq and ChIP-seq data (Figure 6; Supplemental Figures S16 and S18). Based on DAP-seq data, TFs of the TCP, MYB-related, Homeobox/HB, FAR1, and CAMTA families were significantly enriched at photoperiod-responsive ACRs (Supplemental Figure S16). Likewise, binding sites of a selection of flowering-related TFs were enriched at LD-responsive ACRs (Figure 6, A and B). Interestingly, most TFs and TF families were more significantly associated with iACRs in the vasculature, but with rACRs in the epidermis. The CAMTA TF family, which is involved in the coordination of stress responses and includes a Ca^{2+}-regulated Calmodulin binding domain (Shen et al., 2015), represents an exception to this rule (Supplemental Figure S16). This association could be related to the observation that stress-responsive genes are overrepresented among both, differentially expressed genes and iACR-associated genes in the epidermis (Figure 3C; Supplemental Figure S11B).

Tissue-specific TF–TF regulatory networks became obvious when transcriptionally upregulated and iACRs-associated TFs were connected to LD-responsive iACRs containing their respective binding sites (Supplemental Figure S18). Similarly, tissue-specific connectivity was visible in gene regulatory networks based on ChIP-seq data of flowering-related TFs, responsive ACRs, and flowering-related target genes (Figure 6C).

A tissue-specific chromatin-to-expression signature to identify novel flowering time regulators

Based on their strong CC-specific chromatin-to-expression signature we identified *TPS9* as a novel candidate with a potential role in flowering time regulation and confirmed its role based on a late-flowering phenotype of T-DNA and phloem-specific knock-down mutants (Figures 4 and 5). TPS9 is a homolog of TPS1, which activates *FT* expression in leaves and promotes the flowering program in SAM (Wahl et al., 2013). A previous study showed that *TPS9* is expressed in the leaf vasculature (Ramon et al., 2009). *TPS9*, which belongs to the clade II of the *TPS* family, is believed to encode a catalytically nonfunctional trehalose-6-P synthetase, due to a missing catalytic domain. It was suggested that TPS9 plays a role in trehalose monitoring (Ramon et al., 2009). Flowering-related TF bound to the iACR upstream of the *TPS9* promoter (Figure 6). Our analysis exemplifies that gene regulatory networks constructed from cell-type-specific chromatin and expression signatures will help to further dissect flowering time regulation.

The *FT* enhancer *Block C* has been widely investigated to regulate *FT* transcription (Adrian et al., 2010; Cao et al., 2014; Liu et al., 2014; Zicola et al., 2019). Our study adds information on the level of cell-type-specific regulation of chromatin accessibility to further deepen our understanding

of *FT* regulation. An increase in chromatin access in response to LD at *Block C* is observed in the vasculature (Figure 5), which is consistent with increased *FT* mRNA abundance in CCs upon the shift to LDs (Figures 4 and 5). Nevertheless, ACRs at *Block C* are detected in all four experimental conditions, including growth in SD, which corresponds to an absence of *FT* expression. This indicates that *Block C* is constitutively accessible but shows a further increase in chromatin access in correlation with gene expression. Since *Block C* is located at considerable distance from the TSS, an increase in chromatin accessibility is more likely a consequence of transcription factor binding than of increased transcription of the locus. Recently, a second enhancer, *Block E*, participating in LD induction of *FT* expression was identified downstream of the transcription cassette (Zicola et al., 2019), this enhancer is connected to LHY and CDF3 by an rACR overlapping with *Block E* (Figure 6). In the future, it will be interesting to investigate how chromatin chances at both enhancers are coordinated during *FT* induction.

Materials and methods

Plant growth conditions

Two wild-type accessions of *A. thaliana*, Col-0 and L*er* and two INTACT transgenic lines *GAS1p:NTF/ACT2p:BirA*, and *FDHp:NTF/ACT2p:BirA* were used in this study. Plants were cultivated on soil in SDs with a photoperiod cycle of 8-h light/22°C and 16-h darkness/20°C in greenhouse. Then half of the 14 SD plants were moved to long-day-greenhouse (16-h light/22°C and 8-h darkness/20°C) and the other half were kept in SD condition. After extra 3LDs or 3SDs treatment, the plants were collected for INTACT nuclei isolation. Mutants of *tps9-1* (SALK_086992C) and *tps9-2* (SALK_151275C) ordered from NASC were all genotyped as T-DNA homozygous alleles

Plasmid construction

To generate INTACT transgenic line *GAS1p:NTF/ACT2p:BirA*, *GAS1* promoter from entry clone (An et al., 2004) was introduced into *GW::NTF-blue* destination vector (Franziska Turck group, MPIPZ) by gateway LR reaction (Invitrogen, Carlsbad, CA, USA). *GAS1p:NTF* was then transformed into *ACT2p:BirA* Arabidopsis (from Roger Deal Lab, Emory University) mediated by GV3101 agrobacterium. For *FDHp:NTF/ACT2p:BirA* INTACT transgenic line, *FDHp* was first introduced into entry clone, and the following steps as same as generating *GAS1p:NTF/ACT2p:BirA*. For generation of phloem-specific *TPS9* knock-down transgenic plants, *TPS9-amiRNA*#1 and #2 were designed by the amiRNA designer interface WMD3 (Web MicroRNA Designer 3) (http://wmd3.weigelworld.org/cgi-bin/webapp.cgi), integrated into the *MIR319a* backbone (Liang et al., 2012) and cloned into the binary vector SUC2-pGREEN, which was followed by GV3101 *Agrobacterium*-mediated transformation and Basta (BBI Life Science, no.77182-82-2) selection. The primers used in this section are listed in Supplemental Table 2.

INTACT nuclei isolation

INTACT nuclei isolation method is modified from previously described protocol (Deal and Henikoff, 2011; Lu et al., 2017). A 0.5-g plant material of INTACT line (Col-0 background) was mixed with 0.1 g L*er* plants. The above ground part of seedlings cut by scissors is collected on an ice-cooled 60-mm glass plate with 0.5-mL ice-cooled NPB buffer. Chop the samples with a piece of razor blade to release the nuclei which are flitted by a microcloth. M-280 dyna-beads (Thermo Fisher, Waltham, MA, USA) were washed by NPBt buffer. As long as the crude nuclei are released and filtered, 15-μL Dyna-beads are added to mix well with nuclei, followed by adding 0.1% Triton X-100. After rotating the tubes for 45 min at 4°C, transfer the samples into 15-mL tube containing 13-mL NPBt. Enrich the beads conjured nuclei using 15-mL magnet rack and wash the beads conjured nuclei several times. The DAPI-dyed nuclei are tested under the microscope.

Purity test assay

According to the previous method (Moreno-Romero et al., 2017), L*er* as Spike-in material, is mixed with INTACT lines (Col-0 background). Before nuclei purification, an aliquot of suspension was taken as a "Before Sample." After the last washing step of purification, an aliquot of nuclei sample was taken as an "After Sample." Use real-time qPCR to measure a L*er* specific DNA region, *Tα1-2*, in "Before Sample" and "After Sample." *ACT8* is measured as the internal control. INTACT nuclei purity is further calculated.

RNA-seq

Total nuclei RNA was extracted from about 100,000 isolated nuclei using the RNeasy Micro Kit (Qiagen, Hilden, Germany; 74004). cDNA was amplified using the Single Cell Full Length mRNA Amplication Kit (Vazyme, Nanjing, China; N712) according to the user manual. The RNA-seq library of each sample was prepared using TruePrep DNA Library Prep Kit version 2 for Illumina (Vazyme; TD501). The library was purified by the VAHTS DNA Clean Beads (Vazyme; N411) and quantified using Qubit and Agilent 2100 before sequencing by the Illumina HiSeq XTen.

ATAC-seq library

Prepare 50,000 fresh isolated beads conjured nuclei for the consequent ATAC-seq tagmentation (Lu et al., 2017). Convert the buffer from NPBt into tagmentation reaction (Vazyme; TD501) using magnet rack. Incubate the beads conjured nuclei 37°C for 30 min (Bajic et al., 2018). Extract DNA by a CTAB (cetyltrimethylammonium bromide) -chloroform-based method and finally store the DNA water solution at −20°C. Follow the Vazyme TD501 manual to set up ATAC-seq library. Twelve cycles are applied to the PCR step. All these steps above, from material collection until DNA extraction must be executive continuously to ensure the chromatin fresh.

Sequencing information

Sequencing of ATAC- and RNA-seq was performed using the Illumina HiSeq XTen instrument at Novogene. ATAC- and RNA-seq were sequenced in paired-end 150 bp. Information on read counts and alignment statistics can be found in Supplemental Table S1.

ATAC-seq raw data processing and alignment

Raw reads were trimmed with Trimmomatic version 0.36 (Bolger et al., 2014). Reads were trimmed for NexteraPE with a maximum of two seed mismatches, palindrome clip threshold of 30, and simple clip threshold of 10. Reads shorter than 30 bp were discarded. Trimmed reads were aligned to the Arabidopsis TAIR10 reference genome using Bowtie2 version 2.11.1 (Langmead and Salzberg, 2012; Langmead et al., 2019) with the following parameters: "bowtie2 -X 1000." Aligned reads with MAPQ > 10 were sorted using SAMtools version 1.3.1 (Li, 2011; Li et al., 2009) and clonal duplicates were removed using Picard version 2.16.0 (http://broadinstitute.github.io/picard/). PCA of ATAC-seq data using "PlotPCA" in DEseq2 (Love et al., 2014; Kim et al., 2019).

RNA-seq raw data processing, alignment, and expression quantification

Raw reads were trimmed with Trimmomatic version 0.36 (Bolger et al., 2014). Reads were trimmed for Trueseq3 barcodes with a maximum of two seed mismatches, palindrome clip threshold of 30, and simple clip threshold of 10. Reads shorter than 50 bp were discarded. The remaining reads were aligned to the same version reference genome with ATAC-seq using HISAT2 with the parameter "–dta." Raw counts were normalized with DEseq2 to compare gene expression in different samples (Love et al., 2014; Kim et al., 2019). Gene expression values (normalized counts) were calculated by DEseq2. DEGs were also identified with DEseq2 with adjust $P < 0.05$ and fold changes > 2.

Identification of ACRs

ACRs for each tissue were identified with MACS2 (Zhang et al., 2008b). Peaks of each biological sample were called with the "–keep-dup all –extsize 200 –shift 100 -g 1.2e8" and overlapping peaks from both replicates were considered as ACRs. To deal with the variant SPOT in different samples, only reads within ACRs were used to normalize data. In general, ACRs from four cell types were merged and Tn5 integration counts in the merged ACRs (TCM) for each sample were calculated. ACR accessibilities in the eight samples were then normalized to 1 M based for TCMs per sample. ACRs were visualized in the Integrative Genomics Viewer version 2.8.2 (Robinson et al., 2011; Thorvaldsdottir et al., 2013).

Identification of differential i/rACRs

To call differential ACRs, the following filtering steps were performed: Generally, (1) differential ACRs were called with MACS2 (Zhang et al., 2008b) with the "–keep-dup all –extsize 200 –shift 100 -g 1.2e8" by pairwise comparison; (2) the differential peaks from both biological replicates were picked up and overlapped with the samples' ACRs; (3) those differential peaks were further filtered by the Tn5 integration counts which were calculated and normalized based on the strategy detailed above (see "Identification of ACRs" in the above method part); (4) peaks with > 1.5-fold changes and "length > 50 bp" in pairwise comparison were considered as differential ACRs; and (5) cell-type-specific differential ACRs were then identified by comparing different cell types.

Differential ACRs with higher chromatin accessibilities after changing to LD conditions were labeled as induced (i) ACRs while those with lower accessibilities were labeled as repressed (r) ACRs.

Identification of ACR-targeted genes

The target genes of an ACR were identified based on the following strategy: (1) if an ACR was located within −1,000 to + 50 bp of the gene's TSS, it was labeled as the gene's "TSS ACR"; (2) remaining ACRs located in the −50 to + 1,000 bp of the gene's transcriptional end site (TES), were labeled as "TES ACR"; (3) remaining ACRs located in genebodies were labeled as "gene body ACR"; and (4) remaining ACRs were labeled as "Intergenic ACRs" and associated with both, the gene located upstream and downstream.

TF–target gene interaction network

To analyze TF–target gene networks for LD-responsive ACRs, we identified TFBS in different categories of ACRs by finding the overlap between ACRs and published ChIP-seq/DAP-seq peaks. We also use DAP-seq datasets for family-wise enrichment at responsive ACRs of each type. Networks were further built after filtering interactions for iACRs and associated target genes by Cytoscape version 3.7.2 (Otasek et al., 2019). Interactions including known flowering-related TF and target genes were extracted to relate responsive ACRs and DEGs.

GO-term analysis

The panther from TAIR (The Arabidopsis Information Resource) was used for GO (PANTHER version 15.0 software) term enrichment (Mi et al., 2019). The cell-type-specific ACRs associated genes as input and generated representative pathways in biological process.

Identification of enriched motifs

To identify whether responsive ACRs were bound by TF, the overlapping between tissue-specific responsive ACRs and TF DAP-seq peaks (O'Malley et al., 2016) were determined by BEDTools intersect (Quinlan and Hall, 2010). For the analysis, random fragment sets from the non-ACRs regions were used as negative control and all the common ACRs from all four samples were used as positive control. To identify FLM, γFLMβ, and VRN1 floral TF motifs, the ChIP- or DAP-seq binding sites were used for analysis using Discriminative Regular Expression Motif Elicitation (Bailey et al., 2009). The rest floral TF were used DAP-seq or JASPAR dataset (http://jaspar.genereg.net/).

Accession numbers

ATAC- and RNA-seq data have been deposited at NCBI's GEO database (accession number GSE142613). The following secure token has been created to allow review of record GSE142613.

Supplemental data

The following materials are available in the online version of this article.

Supplemental Figure S1. Photoperiodic shift experiments confirm that 3LDs induce early flowering in SD grown Col-0.

Supplemental Figure S2. Tissue-specific marker gene expression in INTACT lines during photoperiodic change.

Supplemental Figure S3. Contamination of ATAC-seq samples with organellar reads.

Supplemental Figure S4. Identification of ACRs.

Supplemental Figure S5. Comparative SPOT analysis of ATAC-seq and DNase-seq datasets.

Supplemental Figure S6. PCA of ATAC-seq data.

Supplemental Figure S7. LD induced and repressed ACRs identified in two biological replicates.

Supplemental Figure S8. Response ACRs in vasculature and epidermis.

Supplemental Figure S9. Representative examples of responsive ACRs.

Supplemental Figure S10. Genomic distribution of responsive ACRs.

Supplemental Figure S11. Cell-type-specific DEGs in vasculature and epidermis.

Supplemental Figure S12. Chromatin accessibility and expression of representative genes showing LD-induction of chromatin access and expression in the vasculature.

Supplemental Figure S13. Identification of *TPS9* mutants.

Supplemental Figure S14. Flowering time of *tps9* mutants in SDs.

Supplemental Figure S15. *TPS9* expression in shoot apices of amiRNA *TPS9* knock-down lines.

Supplemental Figure S16. TF families enriched at LD responsive ACRs.

Supplemental Figure S17. The effect of floral TF enrichment at different categories and gene expression.

Supplemental Figure S18. Regulatory modules of TF-target TF in response to photoperiod.

Supplemental Table S1. Sequencing statistics.

Supplemental Table S2. Primer list.

Supplemental Data Set 1. Leaf phloem and epidermis differential ACRs in response to photoperiod.

Supplemental Data Set 2. GO enrichment in biological process of Differential ACRs.

Supplemental Data Set 3. Leaf phloem and epidermis differentially expressed genes in response to photoperiod.

Supplemental Data Set 4. LD-induced candidate genes in vascular phloem cell.

Supplemental Data Set 5. TF family enrichment based on differential ACRs.

Acknowledgments

We would like to thank members of the Liu lab for discussion and critical reading of the manuscript. We thank Dr Gang Liang for helping design *AtTPS9 amiRNA*. We thank Dr Sarfraz Shafiq for his comments on the manuscript.

Funding

This work was supported by grants from the general program of National Natural Science Foundation of China (grant nos. 31800244 and 31571258 to L.Y.L.), Beijing excellent young scientist program (CIT&TCD201804073), the Youth Innovative Research Team of Capital Normal University (grant no. 010175300900), and the Capacity Building for Sci-Tech Innovation-Fundamental Scientific Research Funds (grant no. 19530050165).

Conflict of interest statement. The authors declare no competing interests.

References

Abdeen A, Miki B (2009) The pleiotropic effects of the bar gene and glufosinate on the Arabidopsis transcriptome. Plant Biotechnol J **7**: 266–282

Adrian J, Farrona S, Reimer JJ, Albani MC, Coupland G, Turck F (2010) cis-Regulatory elements and chromatin state coordinately control temporal and spatial expression of FLOWERING LOCUS T in Arabidopsis. Plant Cell **22**: 1425–1440

Alvarez JM, Moyano TC, Zhang T, Gras DE, Herrera FJ, Araus V, O'Brien JA, Carrillo L, Medina J, Vicente-Carbajosa J, et al. (2019) Local changes in chromatin accessibility and transcriptional networks underlying the nitrate response in Arabidopsis roots. Mol Plant **12**: 1545–1560

An HL, Roussot C, Suarez-Lopez P, Corbesler L, Vincent C, Pineiro M, Hepworth S, Mouradov A, Justin S, Turnbull C, et al. (2004) CONSTANS acts in the phloem to regulate a systemic signal that induces photoperiodic flowering of Arabidopsis. Development **131**: 3615–3626

Andres F, Coupland G (2012) The genetic basis of flowering responses to seasonal cues. Nat Rev Genet **13**: 627–639

Bailey TL, Boden M, Buske FA, Frith M, Grant CE, Clementi L, Ren J, Li WW, Noble WS (2009) MEME SUITE: tools for motif discovery and searching. Nucleic Acids Res **37**: W202–W208

Bajic M, Maher KA, Deal RB (2018) Identification of open chromatin regions in plant genomes using ATAC-Seq. Methods Mol Biol **1675**: 183–201

Bolger AM, Lohse M, Usadel B (2014) Trimmomatic: a flexible trimmer for Illumina sequence data. Bioinformatics **30**: 2114–2120

Bonke M, Thitamadee S, Mahonen AP, Hauser MT, Helariutta Y (2003) APL regulates vascular tissue identity in Arabidopsis. Nature **426**: 181–186

Bouche F, Lobet G, Tocquin P, Perilleux C (2016) FLOR-ID: an interactive database of flowering-time gene networks in Arabidopsis thaliana. Nucleic Acids Res **44**: D1167–D1171

Bourdenx B, Bernard A, Domergue F, Pascal S, Leger A, Roby D, Pervent M, Vile D, Haslam RP, Napier JA, et al. (2011) Overexpression of Arabidopsis ECERIFERUM1 promotes wax very-long-chain alkane biosynthesis and influences plant response to biotic and abiotic stresses. Plant Physiol **156**: 29–45

Brady SM, Orlando DA, Lee JY, Wang JY, Koch J, Dinneny JR, Mace D, Ohler U, Benfey PN (2007) A high-resolution root spatiotemporal map reveals dominant expression patterns. Science **318**: 801–806

Buenrostro JD, Giresi PG, Zaba LC, Chang HY, Greenleaf WJ (2013) Transposition of native chromatin for fast and sensitive epigenomic profiling of open chromatin, DNA-binding proteins and nucleosome position. Nat Methods **10**: 1213–1218

Cao S, Kumimoto RW, Gnesutta N, Calogero AM, Mantovani R, Holt BF, 3rd (2014) A distal CCAAT/NUCLEAR FACTOR Y complex promotes chromatin looping at the FLOWERING LOCUS T promoter and regulates the timing of flowering in Arabidopsis. Plant Cell **26**: 1009–1017

Castillejo C, Pelaz S (2008) The balance between CONSTANS and TEMPRANILLO activities determines FT expression to trigger flowering. Curr Biol **18**: 1338–1343

Cheng Z, Zhang X, Huang P, Huang G, Zhu J, Chen F, Miao Y, Liu L, Fu Y, Wang X (2019) Nup96 and HOS1 are mutually stabilized and gate CONSTANS protein level, conferring long-day photoperiodic flowering regulation in Arabidopsis. Plant Cell **32**: 374–391

Christ B, Hochstrasser R, Guyer L, Francisco R, Aubry S, Hortensteiner S, Weng JK (2017) Non-specific activities of the major herbicide-resistance gene BAR. Nat Plants **3**: 937–945

Collani S, Neumann M, Yant L, Schmid M (2019) FT modulates genome-wide DNA-binding of the bZIP transcription factor FD. Plant Physiol **180**: 367–380

Corbesier L, Vincent C, Jang S, Fornara F, Fan Q, Searle I, Giakountis A, Farrona S, Gissot L, Turnbull C, et al. (2007) FT protein movement contributes to long-distance signaling in floral induction of Arabidopsis. Science **316**: 1030–1033

Deal RB, Henikoff S (2010) A simple method for gene expression and chromatin profiling of individual cell types within a tissue. Dev Cell **18**: 1030–1040

Deal RB, Henikoff S (2011) The INTACT method for cell type-specific gene expression and chromatin profiling in *Arabidopsis thaliana*. Nat Protocol **6**: 56–68

Deng W, Ying H, Helliwell CA, Taylor JM, Peacock WJ, Dennis ES (2011) FLOWERING LOCUS C (FLC) regulates development pathways throughout the life cycle of Arabidopsis. Proc Natl Acad Sci USA **108**: 6680–6685

DeWitt ND, Sussman MR (1995) Immunocytological localization of an epitope-tagged plasma membrane proton pump (H(+)-ATPase) in phloem companion cells. Plant Cell **7**: 2053–2067

Endo M, Shimizu H, Nohales MA, Araki T, Kay SA (2014) Tissue-specific clocks in Arabidopsis show asymmetric coupling. Nature **515**: 419–422

Fornara F, Panigrahi KC, Gissot L, Sauerbrunn N, Ruhl M, Jarillo JA, Coupland G (2009) Arabidopsis DOF transcription factors act redundantly to reduce CONSTANS expression and are essential for a photoperiodic flowering response. Dev Cell **17**: 75–86

Gnesutta N, Kumimoto RW, Swain S, Chiara M, Siriwardana C, Horner DS, Holt BF, 3rd, Mantovani R (2017) CONSTANS imparts DNA sequence specificity to the histone fold NF-YB/NF-YC dimer. Plant Cell **29**: 1516–1532

Haritatos E, Ayre BG, Turgeon R (2000) Identification of phloem involved in assimilate loading in leaves by the activity of the galactinol synthase promoter. Plant Physiol **123**: 929–937

He Y (2009) Control of the transition to flowering by chromatin modifications. Mol Plant **2**: 554–564

Huijser P, Schmid M (2011) The control of developmental phase transitions in plants. Development **138**: 4117–4129

Imaizumi T, Schultz TF, Harmon FG, Ho LA, Kay SA (2005) FKF1 F-box protein mediates cyclic degradation of a repressor of CONSTANS in Arabidopsis. Science **309**: 293–297

Immink RG, Pose D, Ferrario S, Ott F, Kaufmann K, Valentim FL, de Folter S, van der Wal F, van Dijk AD, Schmid M, et al. (2012) Characterization of SOC1's central role in flowering by the identification of its upstream and downstream regulators. Plant Physiol **160**: 433–449

Jacob Y, Mongkolsiriwatana C, Veley KM, Kim SY, Michaels SD (2007) The nuclear pore protein AtTPR is required for RNA homeostasis, flowering time, and auxin signaling. Plant Physiol **144**: 1383–1390

Jiang J (2015) The 'dark matter' in the plant genomes: non-coding and unannotated DNA sequences associated with open chromatin. Curr Opinion Plant Biol **24**: 17–23

Kaufmann K, Wellmer F, Muino JM, Ferrier T, Wuest SE, Kumar V, Serrano-Mislata A, Madueno F, Krajewski P, Meyerowitz EM, et al. (2010) Orchestration of floral initiation by APETALA1. Science **328**: 85–89

Kawakatsu T, Stuart T, Valdes M, Breakfield N, Schmitz RJ, Nery JR, Urich MA, Han X, Lister R, Benfey PN, et al. (2016) Unique cell-type-specific patterns of DNA methylation in the root meristem. Nat Plants **2**: 16058

Kim D, Paggi JM, Park C, Bennett C, Salzberg SL (2019) Graph-based genome alignment and genotyping with HISAT2 and HISAT-genotype. Nat Biotechnol **37**: 907–915

Klemm SL, Shipony Z, Greenleaf WJ (2019) Chromatin accessibility and the regulatory epigenome. Nat Rev Genet **20**: 207–220

Kotake T, Takada S, Nakahigashi K, Ohto M, Goto K (2003) Arabidopsis TERMINAL FLOWER 2 gene encodes a heterochromatin protein 1 homolog and represses both FLOWERING LOCUS T to regulate flowering time and several floral homeotic genes. Plant & Cell Physiol **44**: 555–564

Kumar SV, Lucyshyn D, Jaeger KE, Alos E, Alvey E, Harberd NP, Wigge PA (2012) Transcription factor PIF4 controls the thermosensory activation of flowering. Nature **484**: 242–245

Langmead B, Salzberg SL (2012) Fast gapped-read alignment with Bowtie 2. Nat Methods **9**: 357–359

Langmead B, Wilks C, Antonescu V, Charles R (2019) Scaling read aligners to hundreds of threads on general-purpose processors. Bioinformatics **35**: 421–432

Lee JH, Yoo SJ, Park SH, Hwang I, Lee JS, Ahn JH (2007) Role of SVP in the control of flowering time by ambient temperature in Arabidopsis. Genes Dev **21**: 397–402

Li D, Liu C, Shen L, Wu Y, Chen H, Robertson M, Helliwell CA, Ito T, Meyerowitz E, Yu H (2008) A repressor complex governs the integration of flowering signals in Arabidopsis. Dev Cell **15**: 110–120

Li H (2011) A statistical framework for SNP calling, mutation discovery, association mapping and population genetical parameter estimation from sequencing data. Bioinformatics **27**: 2987–2993

Li H, Handsaker B, Wysoker A, Fennell T, Ruan J, Homer N, Marth G, Abecasis G, Durbin R, Genome Project Data Processing Subgroup. (2009) The sequence alignment/map format and SAMtools. Bioinformatics **25**: 2078–2079

Liang G, He H, Li Y, Yu D (2012) A new strategy for construction of artificial miRNA vectors in Arabidopsis. Planta **235**: 1421–1429

Liu L, Adrian J, Pankin A, Hu J, Dong X, von Korff M, Turck F (2014) Induced and natural variation of promoter length modulates the photoperiodic response of FLOWERING LOCUS T. Nat Commun **5**: 4558

Lopez-Salmeron V, Cho H, Tonn N, Greb T (2019) The phloem as a mediator of plant growth plasticity. Curr Biol **29**: R173–R181

Love MI, Huber W, Anders S (2014) Moderated estimation of fold change and dispersion for RNA-seq data with DESeq2. Genome Biol **15**: 550

Lu Z, Hofmeister BT, Vollmers C, DuBois RM, Schmitz RJ (2017) Combining ATAC-seq with nuclei sorting for discovery of cis-regulatory regions in plant genomes. Nucleic Acids Res **45**: e41

Maher KA, Bajic M, Kajala K, Reynoso M, Pauluzzi G, West D, Zumstein K, Woodhouse M, Bubb KL, Dorrity MW, et al. (2018) Profiling of accessible chromatin regions across multiple plant species and cell types reveals common gene regulatory principles and new control modules. Plant Cell **30**: 15–36

Mateos JL, Madrigal P, Tsuda K, Rawat V, Richter R, Romera-Branchat M, Fornara F, Schneeberger K, Krajewski P, Coupland G (2015) Combinatorial activities of SHORT VEGETATIVE PHASE and FLOWERING LOCUS C define distinct modes of flowering regulation in Arabidopsis. Genome Biol **16**: 31

Mi H, Muruganujan A, Ebert D, Huang X, Thomas PD (2019) PANTHER version 14: more genomes, a new PANTHER GO-slim and improvements in enrichment analysis tools. Nucleic Acids Res **47**: D419–D426

Moreno-Romero J, Santos-Gonzalez J, Hennig L, Kohler C (2017) Applying the INTACT method to purify endosperm nuclei and to generate parental-specific epigenome profiles. Nat Protocol **12**: 238–254

O'Malley RC, Huang SSC, Song L, Lewsey MG, Bartlett A, Nery JR, Galli M, Gallavotti A, Ecker JR (2016) Cistrome and epicistrome features shape the regulatory DNA landscape. Cell **165**: 1280–1292

Oka R, Zicola J, Weber B, Anderson SN, Hodgman C, Gent JI, Wesselink JJ, Springer NM, Hoefsloot HCJ, Turck F, et al. (2017) Genome-wide mapping of transcriptional enhancer candidates using DNA and chromatin features in maize. Genome Biol **18**: 137

Otasek D, Morris JH, Boucas J, Pico AR, Demchak B (2019) Cytoscape automation: empowering workflow-based network analysis. Genome Biol **20**: 185

Pajoro A, Madrigal P, Muino JM, Matus JT, Jin J, Mecchia MA, Debernardi JM, Palatnik JF, Balazadeh S, Arif M, et al. (2014) Dynamics of chromatin accessibility and gene regulation by MADS-domain transcription factors in flower development. Genome Biol **15**: R41

Panikashvili D, Shi JX, Schreiber L, Aharoni A (2009) The Arabidopsis DCR encoding a soluble BAHD acyltransferase is required for cutin polyester formation and seed hydration properties. Plant Physiol **151**: 1773–1789

Pfeiffer A, Shi H, Tepperman JM, Zhang Y, Quail PH (2014) Combinatorial complexity in a transcriptionally centered signaling hub in Arabidopsis. Mol Plant **7**: 1598–1618

Pose D, Verhage L, Ott F, Yant L, Mathieu J, Angenent GC, Immink RG, Schmid M (2013) Temperature-dependent regulation of flowering by antagonistic FLM variants. Nature **503**: 414–417

Potter KC, Wang J, Schaller GE, Kieber JJ (2018) Cytokinin modulates context-dependent chromatin accessibility through the type-B response regulators. Nat Plants **4**: 1102–1111

Pruitt RE, Vielle-Calzada JP, Ploense SE, Grossniklaus U, Lolle SJ (2000) FIDDLEHEAD, a gene required to suppress epidermal cell interactions in Arabidopsis, encodes a putative lipid biosynthetic enzyme. Proc Natl Acad Sci USA **97**: 1311–1316

Putterill J, Laurie R, Macknight R (2004) It's time to flower: the genetic control of flowering time. Bioessays **26**: 363–373

Quinlan AR, Hall IM (2010) BED tools: a flexible suite of utilities for comparing genomic features. Bioinformatics **26**: 841–842

Ramon M, De Smet I, Vandesteene L, Naudts M, Leyman B, Van Dijck P, Rolland F, Beeckman T, Thevelein JM (2009) Extensive expression regulation and lack of heterologous enzymatic activity of the Class II trehalose metabolism proteins from *Arabidopsis thaliana*. Plant Cell Environ **32**: 1015–1032

Reynoso MA, Kajala K, Bajic M, West DA, Pauluzzi G, Yao AI, Hatch K, Zumstein K, Woodhouse M, Rodriguez-Medina J, et al. (2019) Evolutionary flexibility in flooding response circuitry in angiosperms. Science **365**: 1291–1295

Robinson JT, Thorvaldsdottir H, Winckler W, Guttman M, Lander ES, Getz G, Mesirov JP (2011) Integrative genomics viewer. Nat Biotechnol **29**: 24–26

Sawa M, Kay SA (2011) GIGANTEA directly activates flowering locus T in *Arabidopsis thaliana*. Proc Natl Acad Sci USA **108**: 11698–11703

Sawa M, Nusinow DA, Kay SA, Imaizumi T (2007) FKF1 and GIGANTEA complex formation is required for day-length measurement in Arabidopsis. Science **318**: 261–265

Shen C, Yang Y, Du L, Wang H (2015) Calmodulin-binding transcription activators and perspectives for applications in biotechnology. Appl Microbiol Biotechnol **99**: 10379–10385

Sijacic P, Bajic M, McKinney EC, Meagher RB, Deal RB (2018) Changes in chromatin accessibility between Arabidopsis stem cells and mesophyll cells illuminate cell type-specific transcription factor networks. Plant J **94**: 215–231

Sullivan AM, Arsovski AA, Lempe J, Bubb KL, Weirauch MT, Sabo PJ, Sandstrom R, Thurman RE, Neph S, Reynolds AP, et al. (2014) Mapping and dynamics of regulatory DNA and transcription factor networks in A. thaliana. Cell Rep **8**: 2015–2030

Svozil J, Gruissem W, Baerenfaller K (2016) Meselect - a rapid and effective method for the separation of the main leaf tissue types. Front Plant Sci **7**: 1701

Tamaki S, Matsuo S, Wong HL, Yokoi S, Shimamoto K (2007) Hd3a protein is a mobile flowering signal in rice. Science **316**: 1033–1036

Thorvaldsdottir H, Robinson JT, Mesirov JP (2013) Integrative Genomics Viewer (IGV): high-performance genomics data visualization and exploration. Brief Bioinform **14**: 178–192

Truernit E, Sauer N (1995) The promoter of the *Arabidopsis thaliana* SUC2 sucrose-H+ symporter gene directs expression of beta-glucuronidase to the phloem: evidence for phloem loading and unloading by SUC2. Planta **196**: 564–570

Turck F, Fornara F, Coupland G (2008) Regulation and identity of florigen: FLOWERING LOCUS T moves center stage. Ann Rev Plant Biol **59**: 573–594

Usadel B, Blasing OE, Gibon Y, Retzlaff K, Hoehne M, Gunther M, Stitt M (2008) Global transcript levels respond to small changes of the carbon status during progressive exhaustion of carbohydrates in Arabidopsis rosettes. Plant Physiol **146**: 1834–1861

Van de Velde J, Heyndrickx KS, Vandepoele K (2014) Inference of transcriptional networks in Arabidopsis through conserved noncoding sequence analysis. Plant Cell **26**: 2729–2745

Wahl V, Ponnu J, Schlereth A, Arrivault S, Langenecker T, Franke A, Feil R, Lunn JE, Stitt M, Schmid M (2013) Regulation of flowering by trehalose-6-phosphate signaling in *Arabidopsis thaliana*. Science **339**: 704–707

Wang JW, Czech B, Weigel D (2009) miR156-regulated SPL transcription factors define an endogenous flowering pathway in *Arabidopsis thaliana*. Cell **138**: 738–749

Wenkel S, Turck F, Singer K, Gissot L, Le Gourrierec J, Samach A, Coupland G (2006) CONSTANS and the CCAAT box binding complex share a functionally important domain and interact to regulate flowering of Arabidopsis. Plant Cell **18**: 2971–2984

Wu G, Park MY, Conway SR, Wang JW, Weigel D, Poethig RS (2009) The sequential action of miR156 and miR172 regulates developmental timing in Arabidopsis. Cell **138**: 750–759

Yan WH, Chen DJ, Schumacher J, Durantini D, Engelhorn J, Chen M, Carles CC, Kaufmann K (2019) Dynamic control of enhancer activity drives stage-specific gene expression during flower morphogenesis. Nat Commun **10**: 1705

You Y, Sawikowska A, Lee JE, Benstein RM, Neumann M, Krajewski P, Schmid M (2019) Phloem companion cell-specific transcriptomic and epigenomic analyses identify MRF1, a regulator of flowering. Plant Cell **31**: 325–345

You Y, Sawikowska A, Neumann M, Pose D, Capovilla G, Langenecker T, Neher RA, Krajewski P, Schmid M (2017) Temporal dynamics of gene expression and histone marks at the Arabidopsis shoot meristem during flowering. Nat Commun **8**: 15120

Zhang CQ, Barthelson RA, Lambert GM, Galbraith DW (2008a) Global characterization of cell-specific gene expression through fluorescence-activated sorting of nuclei. Plant Physiol **147**: 30–40

Zhang W, Zhang T, Wu Y, Jiang J (2012) Genome-wide identification of regulatory DNA elements and protein-binding footprints using signatures of open chromatin in Arabidopsis. Plant Cell **24**: 2719–2731

Zhang Y, Liu T, Meyer CA, Eeckhoute J, Johnson DS, Bernstein BE, Nusbaum C, Myers RM, Brown M, Li W, et al. (2008b) Model-based analysis of ChIP-Seq (MACS). Genome Biol **9**: R137

Zicola J, Liu L, Tanzler P, Turck F (2019) Targeted DNA methylation represses two enhancers of FLOWERING LOCUS T in *Arabidopsis thaliana*. Nat Plants **5**: 300–307